Supporting information

Room-temperature CO oxidation catalyst: low temperature metal-support interaction between platinum nanoparticles and nanosized Ceria

Suresh Gatla,[†] Daniel Aubert,[‡] Giovanni Agostini,[†] Olivier Mathon,[†] Sakura Pascarelli,*[†] Thomas Lunkenbein,[§] Marc Georg Willinger,[§] Helena Kaper*[‡]

[†]ESRF – The European Synchrotron, 71, avenue des Martyrs, 38000 Grenoble, France

[‡] Ceramic Synthesis and Functionalization Laboratory, UMR 3080, CNRS/Saint-Gobain CREE, 550, Ave Alphonse Jauffret, 84306 Cavaillon, France

[§] Fritz-Haber-Institute of the MPG, Department of Inorganic Chemistry, Faradayweg 4-6, 14195 Berlin

*Correspondence: helena.kaper@saint-gobain.com and sakura@esrf.fr

Contents

Material Preparation

Pure cerium oxide was synthesized by decomposition of cerium nitrate. $Ce(NO_3) \cdot 6H_2O$ (Sigma Aldrich) was dissolved in isopropanol at room temperature. After complete dissolution, the solvent was removed by rotational evaporation at 60 °C until nearly complete dryness. The resulting solid was dried at 100 °C for 48h and crushed in a mortar. The powder was calcined using the following programme: RT-180 °C(2h)-200 °C(3h)-220 °C(3h)-500 °C (2h). Incipient wetness impregnation of cerium oxide was done by mortaring cerium oxide. $Pt(NO_3)_2$ (Heraeus) was dissolved in ethanol and added drop wise to cerium oxide. The obtained powder was dried in an oven at 100 °C for 15h and calcined at 500 °C for 2h under air (ramp: 4°C/min).

Characterization

XRD patterns were recorded on an X'Pert diffractometer from PANanalytical Instruments equipped with a Cu K_α monochromatic radiation source (40 kV, 35 mA). Nitrogen physisorption was carried out at 77K using a Micromeritics Tristar II instrument. Surface areas were calculated using the Brunauer Emmet Teller (BET) method over the range P/P0 = 0.07-0.30, where a linear relationship was maintained. High resolution transmission electron microscopy (HRTEM) micrographs and HAADF-STEM images were recorded on a FEI Titan 80-300 equipped with a Cs corrector.

Catalytic Tests

CO oxidation by molecular oxygen was carried out in a flow-through reactor. The total gas flow was kept constant to 10l/h. The composition of the gas was 6000 ppm of CO and 10 000 ppm of O_2, assuring oxidative conditions during the test. The grain size of the catalyst powder was kept between 150µm and 250µm. 200 mg of catalyst powder was put into the quartz reactor, giving a gas hourly space velocity of 50 000 h-1.

Lattice parameter, crystallite size and surface area

Table S1. Lattice parameter, crystallite size and surface area of the CeO_2 support and, 2.5 wt % Pt/CeO_2 as-prepared and reduced (300 °C/40% H_2) samples.

	Remark	Lattice parameter / (Å)	Crystallite size / (nm)	[a]Surface area / (m^2/g)
CeO_2	Support	5.4125	9	97
2.5 wt %Pt/CeO_2	As-prepared	5.4124	9	82
	Reduced (300°C/40% H_2)	5.4138	9	81

[a] The surface area was determined by using nitrogen physisorption measurements and the Brunauer-Emmett-Teller method (BET).
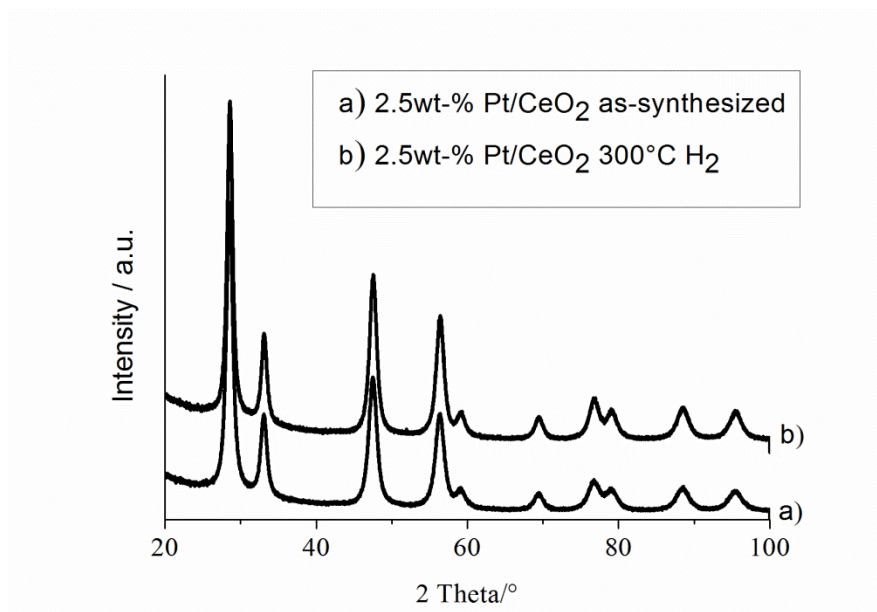
X-Ray Diffraction

Figure S1. XRD pattern of 2.5 wt-% Pt/CeO_2 as-prepared and reduced (300 °C/40% H_2) samples.

HAADF-STEM Analysis
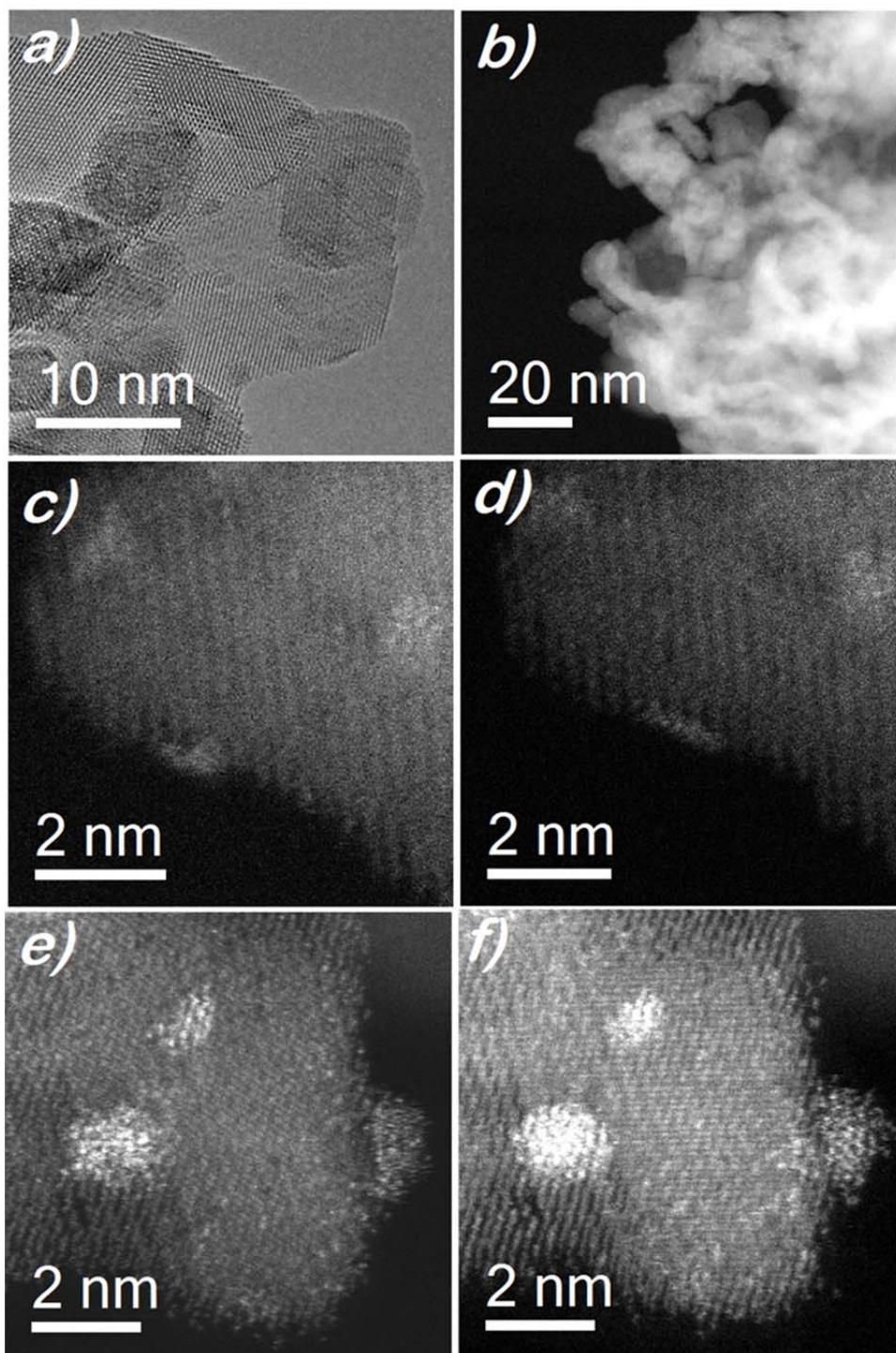
Figure S2. Uncolored (S)TEM images of Pt/CeO$_2$ catalysts. a) HRTEM image of Pt nanoparticles supported on ceria.. b) to d) HAADF-STEM images of Pt/CeO$_2$ catalyst after reductive activation in H$_2$ at different magnifications. c) Atomic resolution HAADF-STEM image and (d) corresponding HAADF-STEM image after exposure to the electron beam for 37 s. e) HAADF-STEM image after CO oxidation and f) HAADF-STEM image of the same position after exposure to the electron beam for 302 s.

Movies M1 and M2 on the behavior of the Pt particles under the electron beam.

M1

M2

Description of XAS measurements

XAS experiments at the Pt L_3-edge (11564 eV) and Ce L_3-edge were performed at the BM23 beamline of the ESRF (Grenoble, France). X-ray absorption spectra for the samples were detected in fluorescence mode, whereas for reference compounds the transmission mode was used. Pt foil, PtO_2, Ce_2O_3 and CeO_2 were measured as references. The oxide samples were pressed into pellets of 13 mm of diameter, using cellulose as binder and diluting agent. In transmission mode, the incoming and transmitted photons were detected by ion chambers I_0 and I_1, respectively. Both ion chambers were filled with required amounts of noble gas to have 30% and 70% absorption on I_0 and I_1 respectively. At the Pt L_3 edge chambers were filled with 0.16 bar and 0.54 bar of Ar for I_0 and I_1 respectively. At the Ce L_3 edge, chambers were filled with 0.45 bar and 1.5 bar of N_2 for I_0 and I_1 respectively. Eventually the pressure in the chambers was raised to 2 bars with He. Figure S3 shows an in-situ cell,[1] developed at ESRF. The sample normal is at an angle of 45° with respect to the incoming X-rays and a 13-element Ge detector collects fluorescence X-rays from the sample at 90° with respect to the incoming X-rays.
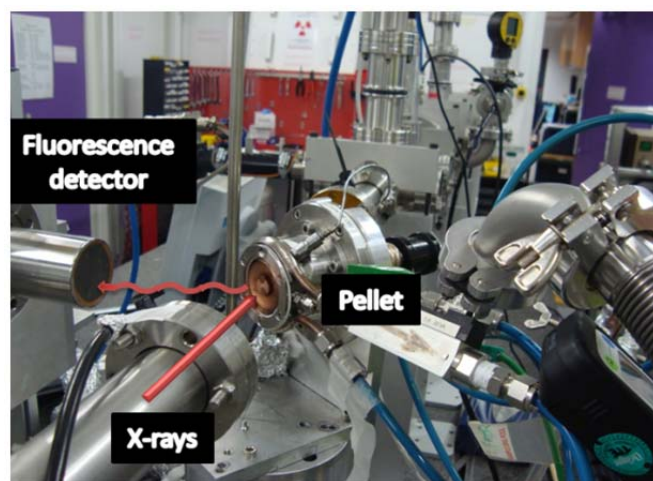
Figure S3. In-situ XAS cell and front end of the 13-element Ge fluorescence detector. In-situ reduction at 300 °C was performed in 5% H_2 and the CO oxidation was done at 50 °C, 100 °C and 150 °C.

A Si(111) double crystal monochromator was used. Harmonic rejection was performed using two Si mirrors at a grazing incidence angle of 2.5 mrad and 4 mrad for Pt L_3 and CeL$_3$, respectively. The photon energy was calibrated using Pt and Cr metal foils for Pt and Ce L_3-edge studies, respectively. The maximum of the first derivative of the EXAFS spectrum was set equal to 11564 eV for the Pt L_3 edge on the Pt foil and equal to 5989 eV for the Cr foil. For each sample, three consecutive EXAFS spectra have been collected and averaged for data analysis. EXAFS parts of the spectra were collected with a constant step in photoelectron wave vector k, with $\Delta k = 0.05$ Å^{-1} up to 12 Å^{-1}. The extraction of the EXAFS $\chi(k)$ function was performed using Athena software and fitting of the EXAFS was performed with Artemis software.[2] Fourier transformation of the k^3 weighted EXAFS function $k^3\chi(k)$ into R space using a Kaiser-Bessel window function was performed in the range 2 to 8 Å^{-1}, yielding the function $|\chi(R)|$ (Å^{-4}). The crystal structure, lattice parameters and space group were taken either from the ATOMS database or ICSD (Inorganic Crystal Structure Database).

The catalyst powder was pressed into 200 mg pellets of 13 mm in diameter and mounted in the cell, before being proceed for in-situ reduction under H_2 (300 °C) and CO oxidation (50 °C, 100 °C and 150 °C). A Eurotherm-2408 was used for precise temperature control. The flow of the gases during the reaction is as follows: He-24.4 ml/min; 2%CO/He-6.6 ml/min; 5%O_2/He-2 ml/min. The concentrations of the CO and O_2 present in the gas feedstock are 2000 ppm and 3000 ppm, which makes 0.2 % and 0.3 % of CO and O_2, respectively.

CO oxidation behavior towards CO_2 was analyzed with a quadrupole mass spectrometer from PFEIFFER. Before starting each experiment, calibration was done for CO and O_2 by recording the corresponding ion current signals. These values were used to calculate the outlet concentrations of CO and O_2. Next to that, CO_2 profiles were recorded with known concentrations i.e 2000, 1000, 500 ppm. All MS profiles were measured using the outlet concentrations.

CO conversion and relative yields and selectivity of CO_2 were calculated quantitatively by calibrating the detected ion current signals of the respective mass fragments at m/z=28 (CO), m/z=41 (CO_2). The conversions of CO and O_2 were calculated based on the following equations.

$$X_{CO} = \frac{[CO]_{inlet} - [CO]_{outlet}}{[CO]_{inlet}} \cdot 100 \text{ \%} \qquad (1)$$

$$X_{[O_2]} = \frac{[O_2]_{inlet} - [O_2]_{outlet}}{[O_2]_{inlet}} \cdot 100 \text{ \%} \qquad (2)$$

Mass spectrometry

CO oxidation behavior towards CO_2 was analyzed with mass spectrometry. CO (2000 ppm) oxidation was performed in the presence of O_2 (3000 ppm) over the as-prepared and in-situ reduced 2.5 wt-% $Pt-CeO_2$ samples at three different temperatures (50 °C, 100 °C and 150 °C). Figure S4 shows the conversion of CO and O_2 over the reduced sample. At all three temperatures, 100% CO conversion and 30% O_2 conversion is reached, which corresponds to a CO:O2 ratio of 2:1, as normally observed for CO oxidation with molecular oxygen.
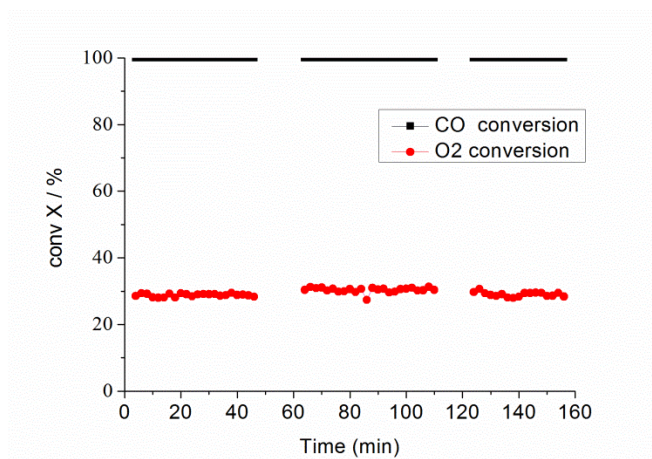

Figure S4. Conversion of CO (X-CO) and O_2 (X-O_2) during the oxidation of 0.2 % CO in presence of 0.3 % O_2 over in-situ reduced 2.5 wt- % $Pt-CeO_2$ samples at three different temperatures (50 °C, 100 °C and 150 °C).

Ce L$_3$-edge FT EXAFS

Figure S5 shows the Ce L$_3$-edge FT EXAFS of the in-situ reduced 2.5 wt-%Pt/CeO$_2$ sample and after CO oxidation at 50 °C, 100 °C and 150 °C. As a comparison, CeO$_2$ reference spectrum and the as-prepared sample are also included. Structural parameters obtained from Ce L$_3$-edge EXAFS are presented in Table S2. As synthesized sample contain Ce-O coordination of 4.2 and is decreased to 3.7 with hydrogen treatment. Further increase in the coordination observed, indicating re-oxidation, during CO oxidation.
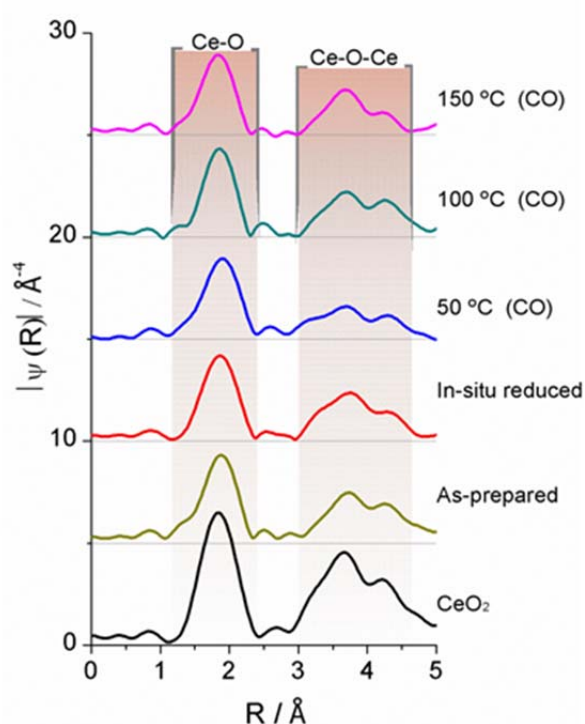
Figure S5. Fourier transformed Ce L$_3$-edge EXAFS spectra of the in-situ reduced 2.5 wt % Pt/CeO$_2$ sample measured while CO oxidation at three different temperatures (50 °C, 100 °C and 150 °C). As comparison, spectra of CeO$_2$ and as-prepared 2.5 wt-% Pt/CeO$_2$ sample are shown.

Table S2. Structural parameters obtained from Ce L$_3$-edge EXAFS of as-prepared and in-situ reduced 2.5 wt-% Pt-CeO$_2$ catalyst measured during CO oxidation at three different temperatures (50 °C, 100 °C and 150 °C)

Sample	Treatment	Shell	N	R(Å)	σ^2(Å^{-2})	ΔEo / eV
CeO$_2$		Ce-O	6.8 ± 2.0	2.32 ± 0.03	0.009 ± 0.004	7 ± 3
Pt/CeO$_2$	As synthesized	Ce-O	4.2 ± 0.9	2.32 ± 0.02	0.008 ± 0.003	7 ± 2

Reduced 300 °C/H$_2$	Ce-O	3.7 ± 0.7	2.32 ± 0.01	0.007 ± 0.003	7 ± 1
CO oxidation-50 °C	Ce-O	4 ± 2	2.34 ± 0.04	0.006 ± 0.005	8± 4
CO oxidation-100 °C	Ce-O	4.5 ± 0.7	2.31 ± 0.01	0.005 ± 0.003	7 ± 1
CO oxidation-150 °C	Ce-O	4.6 ± 0.8	2.30 ± 0.01	0.011 ± 0.003	6± 1

Pt L$_3$-edge XANES

In this part, the effect of CO oxidation on the XANES of the in-situ reduced 2.5 wt % Pt/CeO$_2$ sample is discussed and comparison is made with the as-prepared sample. Normalized Pt L$_3$-edge XANES and the corresponding first derivative are presented in Figure S6. The white line intensity of the in-situ reduced sample is lower than the as-synthesized sample, and is comparable to that in metallic Pt. This is consistent with the higher filling of the d-orbitals of Pt after reduction, and suggests the presence of metallic Pt species. But the E$_0$ (from first derivatives) value of the data relative to the in-situ reduced sample appears to be 0.6 eV higher than the value observed for metallic Pt (11564 eV). This energy shift could be caused by the presence of low temperature metal-support interactions between metallic Pt and CeO$_2$ through the possible oxygen linkage.

Further, during CO oxidation, the white line intensity gradually increases and the peak position shifts to higher energy with increasing reaction temperature, which indicates a partial particle oxidation. Safonova et al. claimed that the increase in the white line intensity, especially under CO exposure, can also be due to overlapping of the d-orbitals of Pt metal with the 2π* orbitals of the C and O atoms, forming an anti-bonding state above the Fermi level.[3]
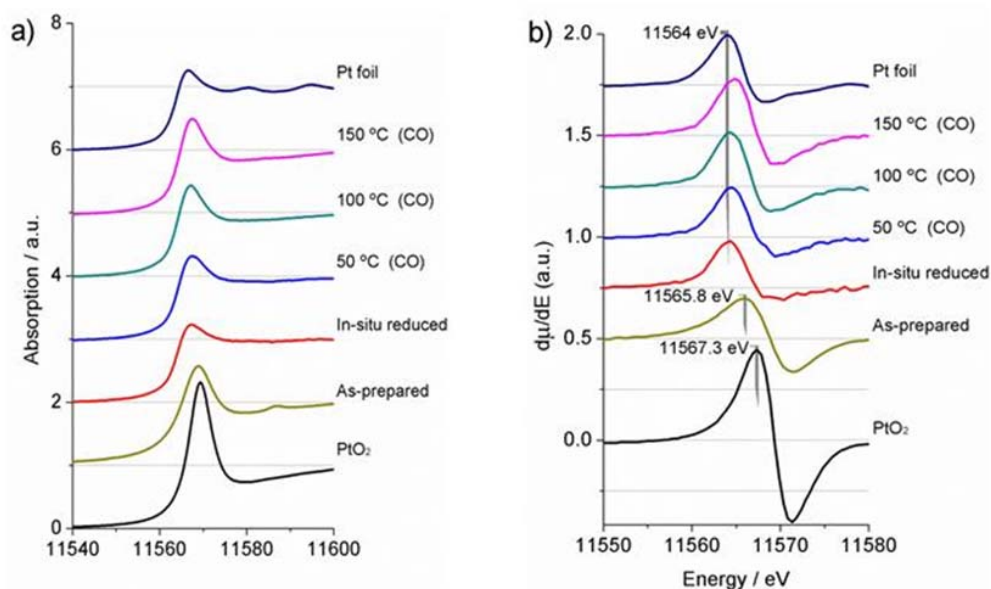
Figure S6. a) Normalized Pt L_3-edge XANES spectra of the in-situ reduced 2.5 wt % Pt/CeO$_2$ sample measured during CO oxidation at three different temperatures (50 °C, 100 °C and 150 °C), b) first derivative curves of XANES. As a comparison, spectra of PtO$_2$, Pt foil and as-prepared 2.5 wt-% Pt/CeO$_2$ sample are presented.

Structural parameters obtained from Pt L_3-edge EXAFS analysis

Table S3. Structural parameters obtained from Pt L_3-edge EXAFS of Pt-metal and PtO$_2$.

Sample	Shell	N	R(Å)	$\sigma^2(Å^{-2})$	ΔEo / eV
PtO$_2$	Pt-O	4.8 ± 0.6	2.00 ± 0.01	0.003 ± 0.001	11 ± 1
	Pt-Pt	4.8	3.08 ± 0.01	0.008 ± 0.004	
Pt foil	Pt-Pt	12.0	2.764 ± 0.002	0.005 ± 0.001	9 ± 1
	Pt-Pt	6.0	3.92 ± 0.01	0.007 ± 0.001	

Table S4. Structural parameters obtained from Pt L_3-edge EXAFS of the as-synthesized and in-situ reduced 2.5 wt-% Pt/CeO_2 catalyst measured during CO oxidation at three different temperatures (50 °C, 100 °C and 150 °C).

Treatment	Shell	N	R(Å)	$\sigma^2(Å^{-2})$	ΔEo / eV
As-prepared	Pt-O	2.9 ± 0.4	2.009 ± 0.009	0.002 ± 0.001	14 ± 2
	Pt-Pt	2.9	3.17 ± 0.06	0.019 ± 0.008	
Reduced 300 °C/H$_2$	*Pt-Pt	5.3 ± 3.0	2.72 ± 0.01	0.009 ± 0.005	8.5
	Pt-O	1.0 ± 0.2	2.10 ± 0.05	0.004	14 ± 4
CO oxidation-50	*Pt-Pt	8 ± 3	2.72 ± 0.01	0.014 ± 0.005	8.5
	Pt-O	1.3 ± 0.2	2.10 ± 0.03	0.003	13 ± 3
CO oxidation-100	*Pt-Pt	3.0 ± 1.0	2.70 ± 0.04	0.008 ± 0.003	8.5
	Pt-O	1.8 ± 0.8	2.03 ± 0.03	0.0004 ± 0.006	13 ± 4
CO oxidation-150	*Pt-Pt	1.3 ± 0.6	2.69 ± 0.03	0.001 ± 0.005	8.5
	Pt-O	2.2 ± 0.8	2.01 ± 0.044	0.003	11 ± 3

* Pt metal contribution

Table S3 contains structural parameters of Pt-metal and PtO_2 obtained from Pt L_3-edge EXAFS and Table S4 represents as-synthesized 2.5 wt-% Pt/CeO_2 catalyst, in-situ reduced sample and after subsequent CO oxidation at 50 °C, 100 °C and 150 °C. The Pt-O distance observed in as-synthesized 2.5 wt-% Pt/CeO_2 is close to the value in the PtO_2 reference. However, the Pt-O bond distance found in the reduced sample or after CO oxidation at 50 °C is significantly longer, indicating prominent interaction of Pt with CeO_2. The Pt-O distance in other samples is more similar to that in PtO_2. This can be due to the fact that some platinum remains in the favorable situation of sharing oxygen with cerium oxide (long bond), while platinum on the surface of the nanoparticles oxidizes (short bond). Thus, EXAFS provided average values over all Pt-O distances in the samples. We also observe that the reduction treatment increases the relative amount of metallic Pt (CN of 5.3), while coordination number decreases upon CO oxidation.

XANES Simulations – FMS variation and broadening

We performed ab initio full multiple scattering (FMS) simulations of the Pt L_3 XANES spectra of the PtO_2, and the as-prepared and the in-situ reduced 2.5 wt %/CeO_2

sample, using the FEFF9 code.[4] The muffin-tin and the Hedin-Lundquist exchange correlation potentials were used. An atomic cluster of 70 atoms was sufficient to reproduce the main features of the experimental data. Different atomic configurations were tested for the two samples. Best results were obtained by using:

i)   for the as-prepared sample, the PtO structure is considered, where Pt is coordinated with 4 oxygen atoms. The distance between Pt to O is considered as 2.01 Å.

ii) for the in-situ reduced sample, the atomic configuration shown in Figure 4 depicting a Pt_4 cluster lying on top of the CeO_2(111) surface, with the three base Pt atoms bonded to oxygen atoms at a distance of 2.10 Å

We only look at the first shell in the Pt-O model. From our experience, the possible presence of other atoms such as H would not affect the EXAFS signal and are thus not relevant in this study.[5]

Different FMS cluster sizes were tested. We find convergence for an FMS cluster size of 5 Å. A 1 eV broadening was added using the EXCHANGE card.

Surface defects are often cited as contributing to the catalytic activity. To see whether our simulation of the XAFS measurements are influenced by the presence of defects, we considered thus the presence of Ce^{3+} cations as a source of defects in the form of oxygen ion vacancies, as par exemple stated by Bruix et al.[6] By the same authors, it was also shown that for reduced CeO2-x models, oxygen ions were back transferred onto the Pt particles. We thus repeated simulation considering three different situations, 100% Ce4+, 20% Ce3+ and 30% Ce3+. As can be seen in Figure S7, the white line intensity of the Pt absorption edge decreases only slightly thus demonstrating that in this special case, ceria defects can be neglected.
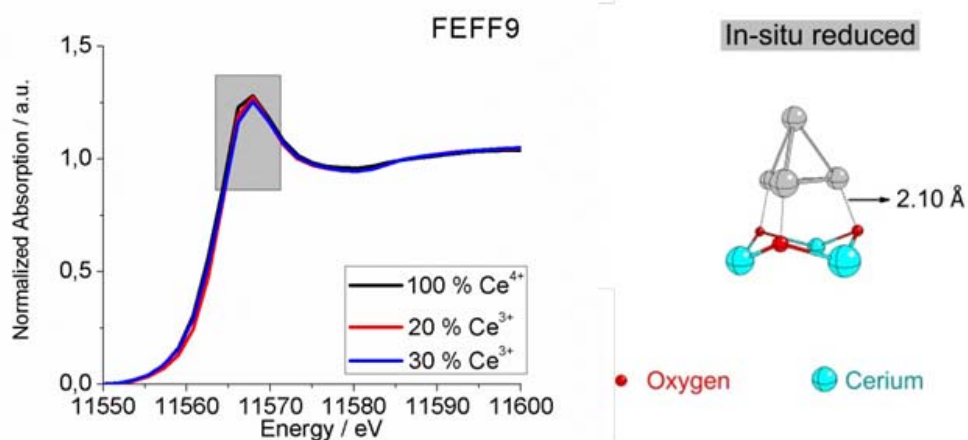
Figure S7. Simulated XANES patterns (left panel) with FEFF9 code based on the proposed model structures (right) panel). 100 % Ce^{4+}, 20 %Ce^{3+} and 30%Ce^{3+} were considered for the simulations. Different radios of Ce were obtained by introducing ION card in the FEFF input file.

Input file to FEFF9 for the calculation of XANES of in-situ reduced 2.5 wt %Pt/CeO_2

TITLE Pt1 top in model fms 5

EDGE L3
S02 1.0

CONTROL 1 1 1 1 1 1

PRINT 0 0 0 0 0 0

EXCHANGE 0 0.0 1.0 -1
SCF 4.0 0 100 0.2 1
COREHOLE FSR
XANES 4.0 0.07 0.0
FMS 5 0

POTENTIALS
0 78 Pt -1 3 0.001
1 78 Pt -1 3 0.01

2 8 O   -1 2 2.0
3 58 Ce -1 3 1.0

ATOMS
 0.00000 0.00000 0.00000 0 Pt 0.00000 0
-0.93425 -2.20067 -1.25992 1 Pt 2.70244 1
-0.44319 -2.31521 1.32125 1 Pt 2.70228 2
 1.54810 -2.18002 -0.39146 1 Pt 2.70228 3
-0.62100 -4.33514 1.87643 2 O   4.76445 4
 2.27887 -4.13826 -0.61775 2 O   4.76445 5
-1.33630 -4.16833 -1.88268 2 O   4.76499 6
 1.56921 -5.02827 1.42754 3 Ce 5.45745 7
-2.04459 -5.05839 0.16419 3 Ce 5.45844 8
 0.85907 -4.86125 -2.33323 3 Ce 5.46019 9

END

ITLE Pt2 side in model fms 5

EDGE L3

S02 1.0

CONTROL 1 1 1 1 1 1

PRINT 0 0 0 0 0 0

EXCHANGE 0 0.0 1.0 -1

SCF 4.0 0 100 0.2 1

COREHOLE FSR

XANES 4.0 0.07 0.0

FMS 5 0

POTENTIALS

0 78 Pt -1 3 0.001

1 78 Pt -1 3 0.01

2 8 O   -1 2 2.0

3 58 Ce -1 3 1.0

ATOMS

```
 0.00000  0.00000  0.00000  0 Pt  0.00000  0
-0.49105  0.11454 -2.58117  1 Pt  2.62996  1
 1.99129  0.13519 -1.71271  1 Pt  2.63000  2
 0.44319  2.31521 -1.32125  1 Pt  2.70228  3
-0.17781 -2.01993  0.55518  2 O   2.10237  4
 2.72206 -1.82305 -1.93900  2 O   3.80695  5
-0.89310 -1.85312 -3.20393  2 O   3.80748  6
 2.01240 -2.71306  0.10629  3 Ce  3.37961  7
-1.60139 -2.74318 -1.15706  3 Ce  3.38057  8
 1.30226 -2.54604 -3.65449  3 Ce  4.64042  9
```

END

Input file to FEFF9 for the calculation of XANES of as-synthesized 2.5 wt %Pt/CeO₂

TITLE Pt1O1 fms 5

EDGE L3

S02 1.0

CONTROL 1 1 1 1 1 1

PRINT 0 0 0 0 0 0

EXCHANGE 0 0.0 1.0 -1

SCF 4.0 0 100 0.2 1

COREHOLE FSR

XANES 4.0 0.07 0.0

FMS 5 0

POTENTIALS

0 78 Pt -1 3 0.001

1 78 Pt -1 3 1

2 8 O -1 2 1

ATOMS

0.00000	0.00000	0.00000	0 Pt	0.00000
1.53885	0.00000	1.33500	2 O	2.03722
-1.53885	0.00000	1.33500	2 O	2.03722
1.53885	0.00000	-1.33500	2 O	2.03722
-1.53885	0.00000	-1.33500	2 O	2.03722
3.07770	0.00000	0.00000	1 Pt	3.07770
-3.07770	0.00000	0.00000	1 Pt	3.07770
0.00000	3.07770	0.00000	1 Pt	3.07770
0.00000	-3.07770	0.00000	1 Pt	3.07770
1.53885	1.53885	2.67000	1 Pt	3.44456

-1.53885	1.53885	2.67000	1 Pt	3.44456
1.53885	-1.53885	2.67000	1 Pt	3.44456
-1.53885	-1.53885	2.67000	1 Pt	3.44456
1.53885	1.53885	-2.67000	1 Pt	3.44456
-1.53885	1.53885	-2.67000	1 Pt	3.44456
1.53885	-1.53885	-2.67000	1 Pt	3.44456
-1.53885	-1.53885	-2.67000	1 Pt	3.44456
1.53885	3.07770	1.33500	2 O	3.69087
-1.53885	3.07770	1.33500	2 O	3.69087
1.53885	-3.07770	1.33500	2 O	3.69087
-1.53885	-3.07770	1.33500	2 O	3.69087
1.53885	3.07770	-1.33500	2 O	3.69087
-1.53885	3.07770	-1.33500	2 O	3.69087
1.53885	-3.07770	-1.33500	2 O	3.69087
-1.53885	-3.07770	-1.33500	2 O	3.69087
1.53885	0.00000	4.00500	2 O	4.29046
-1.53885	0.00000	4.00500	2 O	4.29046
1.53885	0.00000	-4.00500	2 O	4.29046
-1.53885	0.00000	-4.00500	2 O	4.29046
3.07770	3.07770	0.00000	1 Pt	4.35253
-3.07770	3.07770	0.00000	1 Pt	4.35253
3.07770	-3.07770	0.00000	1 Pt	4.35253
-3.07770	-3.07770	0.00000	1 Pt	4.35253
4.61655	0.00000	1.33500	2 O	4.80570
-4.61655	0.00000	1.33500	2 O	4.80570
4.61655	0.00000	-1.33500	2 O	4.80570
-4.61655	0.00000	-1.33500	2 O	4.80570
1.53885	3.07770	4.00500	2 O	5.28018

-1.53885	3.07770	4.00500	2 O	5.28018
1.53885	-3.07770	4.00500	2 O	5.28018
-1.53885	-3.07770	4.00500	2 O	5.28018
1.53885	3.07770	-4.00500	2 O	5.28018
-1.53885	3.07770	-4.00500	2 O	5.28018
1.53885	-3.07770	-4.00500	2 O	5.28018
-1.53885	-3.07770	-4.00500	2 O	5.28018
0.00000	0.00000	5.34000	1 Pt	5.34000
0.00000	0.00000	-5.34000	1 Pt	5.34000
4.61655	1.53885	2.67000	1 Pt	5.55063
-4.61655	1.53885	2.67000	1 Pt	5.55063
1.53885	4.61655	2.67000	1 Pt	5.55063
-1.53885	4.61655	2.67000	1 Pt	5.55063
4.61655	-1.53885	2.67000	1 Pt	5.55063
-4.61655	-1.53885	2.67000	1 Pt	5.55063
1.53885	-4.61655	2.67000	1 Pt	5.55063
-1.53885	-4.61655	2.67000	1 Pt	5.55063
4.61655	1.53885	-2.67000	1 Pt	5.55063
-4.61655	1.53885	-2.67000	1 Pt	5.55063
1.53885	4.61655	-2.67000	1 Pt	5.55063
-1.53885	4.61655	-2.67000	1 Pt	5.55063
4.61655	-1.53885	-2.67000	1 Pt	5.55063
-4.61655	-1.53885	-2.67000	1 Pt	5.55063
1.53885	-4.61655	-2.67000	1 Pt	5.55063
-1.53885	-4.61655	-2.67000	1 Pt	5.55063
4.61655	3.07770	1.33500	2 O	5.70675
-4.61655	3.07770	1.33500	2 O	5.70675
4.61655	-3.07770	1.33500	2 O	5.70675

```
-4.61655  -3.07770   1.33500  2 O          5.70675

 4.61655   3.07770  -1.33500  2 O          5.70675

-4.61655   3.07770  -1.33500  2 O          5.70675

 4.61655  -3.07770  -1.33500  2 O          5.70675

-4.61655  -3.07770  -1.33500  2 O          5.70675
```

END

References

(1)   Guilera, G.; Gorges, B.; Pascarelli, S.; Vitoux, H.; Newton, M. a.; Prestipino, C.; Nagai, Y.; Hara, N. *J. Synchrotron Radiat.* **2009**, *16*, 628–634.

(2)   Ravel, B.; Newville, M. *J. Synchrot. Radiat.* **2005**, *12*, 537–541.

(3)   Safonova, O.; Tromp, M.; Bokhoven, J. A.; Groot, F. M. F.; Evans, J.; Glatzel, P. *J. Phys. Chem. B* **2006**, *110*, 16162–16164.

(4)   Ankudinov, A. L.; Ravel, B.; Rehr, J. J.; Conradson, S. D. *Phys. Rev. B Condens. Mater. Phys.* **1998**, *58*, 7565–7576.

(5)   Agostini, G.; Groppo, E.; Piovano, A.; Pellegrini, R.; Leofanti, G.; Lamberti, C. *Langmuir* **2010**, *26*, 11204–11211.

(6)   Bruix, A.; Migani, A.; Vayssilov, G. N.; Neyman, K. M.; Libuda, J.; Illas, F. *Phys. Chem. Chem. Phys.* **2011**, *13*, 11384–11392.